The Astronomical Journal, 124:690–705, 2002 August
© 2002. The American Astronomical Society. All rights reserved. Printed in U.S.A.

A CATALOG OF H I–SELECTED GALAXIES FROM THE SOUTH CELESTIAL CAP REGION OF SKY

V. A. Kilborn,[1,2] R. L. Webster,[1] L. Staveley-Smith,[3] M. Marquarding,[3] G. D. Banks,[4] D. G. Barnes,[5] R. Bhathal,[6] W. J. G. de Blok,[3] P. J. Boyce,[7] M. J. Disney,[4] M. J. Drinkwater,[1] R. D. Ekers,[3] K. C. Freeman,[8] B. K. Gibson,[5] P. A. Henning,[9] M. Howlett,[5] H. Jerjen,[8] P. M. Knezek,[10,11] B. Koribalski,[3] D. F. Malin,[12] R. F. Minchin,[4] J. R. Mould,[8] J. C. O'Brien,[8] T. Oosterloo,[13] P. F. Ortiz,[14] R. M. Price,[3,9] M. E. Putman,[15] S. D. Ryder,[12] E. M. Sadler,[16] I. M. Stewart,[17] F. Stootman,[6] O. I. Wong,[1] and A. E. Wright[3]

Received 2001 December 14; accepted 2002 March 29

ABSTRACT

The first deep catalog of the H I Parkes All Sky Survey (HIPASS) is presented, covering the south celestial cap (SCC) region. The SCC area is ~2400 deg^2 and covers $\delta < -62°$. The average rms noise for the survey is 13 mJy beam^{-1}. Five hundred thirty-six galaxies have been cataloged according to their neutral hydrogen content, including 114 galaxies that have no previous cataloged optical counterpart. This is the largest sample of galaxies from a blind H I survey to date. Most galaxies in optically unobscured regions of sky have a visible optical counterpart; however, there is a small population of low-velocity H I clouds without visible optical counterparts whose origins and significance are unclear. The rms accuracy of the HIPASS positions is found to be 1$'$.9. The H I mass range of galaxies detected is from ~10^6 to ~10^{11} $M_\odot$. There are a large number of late-type spiral galaxies in the SCC sample (66%), compared with 30% for optically selected galaxies from the same region in the NASA Extragalactic Database. The average ratio of H I mass to B luminosity of the sample increases according to optical type, from 1.8 $M_\odot/L_\odot$ for early types to 3.2 $M_\odot/L_\odot$ for late-type galaxies. The H I–detected galaxies tend to follow the large-scale structure traced by galaxies found in optical surveys. From the number of galaxies detected in this region of sky, we predict the full HIPASS catalog will contain ~5000 galaxies, to a peak flux density limit of ~39 mJy (3 σ), although this may be a conservative estimate as two large voids are present in the region. The H I mass function for this catalog is presented in a subsequent paper.

Key words: catalogs — galaxies: general — surveys

On-line material: machine-readable table

1. INTRODUCTION

Galaxy evolution is largely driven by the gravitational collapse of overdense regions, and the conversion of gas into stars. At the present epoch, much gas has already been converted into stellar material, although significant quantities remain in the interstellar and intergalactic medium. The largest amount is probably ionized and locked up in the diffuse and warm or hot phases of the intergalactic medium (Davé et al. 2001). However, the cooler, neutral component can more easily condense into stars and galaxies. A direct way of measuring the remaining neutral component, irrespective of the brightness of any accompanying starlight, is through detection of the 21 cm H I line. The H I line is able to reveal primordial gas clouds yet to condense into stars and gas associated with star-forming galaxies, as well as gas resulting from the photodissociation of molecular hydrogen in regions of intense UV radiation (Smith et al. 2000; Allen 2001).

The H I content of galaxies depends to a degree on the environment in which the galaxy resides (Haynes, Giovanelli, & Chincarini 1984). Galaxies near the center of clusters are likely to be H I deficient (Solanes et al. 2001; Giovanalli & Haynes 1985), while gas removal effects are not as acute in low-density regions and smaller galaxy groups (Huchtmeier, Hopp, & Kuhn 1997; Valluri & Jog 1991). The H I content of galaxies also varies according to their Hubble type. H I is predominately found in spiral galaxies (Rao & Briggs 1993; Hoffman et al. 1989), and Solanes, Giovanelli, & Haynes (1996) found that Sb galaxies generally had a higher H I mass compared with other spiral

[1] School of Physics, University of Melbourne, Parkville, Victoria 3010, Australia.
[2] Jodrell Bank Observatory, University of Manchester, Macclesfield, Cheshire SK11 9DL, UK; vkilborn@jb.man.ac.uk.
[3] Australia Telescope National Facility, CSIRO, P.O. Box 76, Epping, NSW 1710, Australia.
[4] Department of Physics and Astronomy, University of Wales, Cardiff, P.O. Box 913, Cardiff CF24 3YB, UK.
[5] Swinburne University of Technology, Mail Number 31, P.O. Box 218, Hawthorn, Victoria 3122, Australia.
[6] Department of Physics, University of Western Sydney Macarthur, P.O. Box 555, Campbelltown, NSW 2560, Australia.
[7] Department of Physics, University of Bristol, Tyndall Avenue, Bristol BS8 1TL, UK.
[8] Research School of Astronomy and Astrophysics, Australian National University, Weston Creek Post Office, Weston, ACT 2611, Australia.
[9] Department of Physics and Astronomy, University of New Mexico, 800 Yale Boulevard, NE, Albuquerque, NM 87131.
[10] WIYN Consortium, Inc., 950 North Cherry Avenue, Tucson, AZ 85726.
[11] Visiting Astronomer, Cerro Tololo Inter-American Observatory, National Optical Astronomy Observatory, which is operated by the Association of Universities for Research in Astronomy, Inc., under cooperative agreement with the National Science Foundation.
[12] Anglo-Australian Observatory, P.O. Box 296, Epping, NSW 1710, Australia.
[13] Netherlands Foundation for Research in Astronomy, P.O. Box 2, 7990 AA Dwingeloo, Netherlands.
[14] Osservatorio Astronomico di Capodimonte, via Moiariello 16, I-80131 Naples, Italy.
[15] Center for Astrophysics and Space Astronomy, University of Colorado, Campus Box 389, Boulder, CO 80309.
[16] Department of Astrophysics, School of Physics, University of Sydney, A28, Sydney, NSW 2006, Australia.
[17] Department of Physics and Astronomy, University of Leicester, University Road, Leicester LE1 7RH, UK.

galaxies. The H I content of dwarf galaxies varies with their morphology. Low-luminosity irregular dwarfs are typically H I–rich, while dwarf spheroidal and elliptical galaxies are rarely detected in neutral hydrogen (Carignan 1999; Kraan-Korteweg & Tamman 1979). Low surface brightness (LSB) galaxies are typically H I–rich, and the H I content of LSB dwarf galaxies increases with decreasing optical luminosity (Staveley-Smith, Davies, & Kinman 1992). The H I content of E and S0 galaxies is low, with only 10%–15% of these galaxies typically detected in neutral hydrogen. It is commonly thought that the majority of the H I seen in these galaxies is from recent or past accretion from a gas-rich companion, as the H I distribution is typically irregular (Duprie & Schneider 1996). However, there is evidence of a small population of low-luminosity early-type galaxies and dwarf elliptical galaxies that have an intrinsic content of neutral hydrogen (Oosterloo & Morganti 2001; Sadler 1997), suggesting these galaxies had a different evolutionary path to more luminous, H I-poor elliptical galaxies.

The neutral hydrogen (H I) content of the local universe has hitherto largely been determined using H I observations based on optical or infrared catalogs of galaxies. However, optical catalogs are biased against galaxies of low optical surface brightness (Impey & Bothun 1997; Disney 1976), so that a substantial part of the possibly H I–rich galaxy population is missed in such surveys. To obtain a thorough census of the neutral hydrogen in the local universe, blind H I surveys are necessary. Although previous blind H I surveys have covered a range of large-scale structure, the total area surveyed so far is low. The most recent, and largest, blind surveys by Sorar (1994), Spitzak & Schneider (1998), and Rosenberg & Schneider (2000) looked at a range of right ascension at particular declinations, thus enabling a variety of environments to be probed. The number statistics are low, with 65, 75, and 265 galaxies detected, respectively. The galaxies follow the same large-scale structure as galaxies detected optically in the same regions. Sorar (1994) and Spitzak & Schneider (1998) found optical counterparts to all their H I detections, and Rosenberg & Schneider (2000) find that most of their detections have an optical counterpart, although some have very low surface brightness. In addition, blind H I surveys have been conducted through the optically obscured zone of avoidance (ZOA; Henning et al. 2000). Such surveys are important in determining the local large-scale structure, which is impossible to do optically in this region (Juraszek et al. 2000). Including these recent ZOA surveys, no population of galaxies has been detected in H I that has significantly increased the calculated H I mass density of the local universe.

The distribution of H I in the local universe will soon be known better than ever before, because of the completion of the largest ever survey for H I, the H I Parkes All-Sky Survey (HIPASS). HIPASS has produced some exciting results even in the early stages of analysis, including the discovery of 10 new members of the Centaurus A Group (Banks et al. 1999), an H I cloud at low velocity (Kilborn et al. 2000), and an H I cloud associated with NGC 2442 (Ryder et al. 2001). This paper describes the first catalog produced from ~11% of the HIPASS survey region. This region covers an area of 2400 deg^2 in the south celestial cap (SCC). The catalog contains 536 galaxies, ranging in mass from $M_{\rm H\,I} \sim 10^6$ to $M_{\rm H\,I} \sim 10^{11}$ $M_\odot$ (H_0 of 75 km s^{-1} Mpc^{-1} is assumed throughout). While recent surveys have been concentrating on increasing the number statistics of low-mass galaxies, this sample occupies a large volume, which also enables the increase of statistics on high-mass galaxies. The mass limit of the survey is approximately $M_{\rm H\,I} \sim 10^6 D^2_{\rm Mpc}$ $M_\odot$, assuming a line width of 100 km s^{-1}, so the lowest-mass galaxies lie within a few megaparsecs. The catalog contains 16 galaxies of low H I mass ($M_{\rm H\,I} \lesssim 10^8$ $M_\odot$) and seven galaxies with an H I mass larger than 3×10^{10} $M_\odot$. Higher resolution H I observations were made for a number of detections. These observations, as well as the general properties of the sample, will be discussed in this paper.

The survey parameters are given in § 2, and the catalog and selection criteria are described in § 3. The accuracies of the HIPASS derived parameters are explored in § 4. The completeness and reliability of the sample are discussed in § 5. The characteristics of galaxies detected in the survey are presented in § 6, and the spatial distribution is compared with optically known large-scale structure in § 7. The properties of the new H I galaxies are explored in § 8, and finally a summary and predictions for the full survey are presented in § 9. Throughout the paper, the quoted velocities are heliocentric velocities (cz), unless otherwise indicated.

2. SURVEY PARAMETERS

HIPASS surveyed the whole southern sky in H I to declination $\delta < +2^\circ$ and is presently continuing to the north, to $\delta < +25^\circ$. A complementary survey, the H I Jodrell All-Sky Survey (HIJASS) is continuing northward from $\delta > +25^\circ$ (Boyce et al. 2001). The HIPASS survey uses the multibeam 13-beam receiver mounted on the Parkes telescope.[18] A 64 MHz bandpass with 1024 channels is used, which gives velocity coverage from −1200 to 12,700 km s^{-1}. The data are bandpass-corrected and gridded into $8^\circ \times 8^\circ$ cubes (Barnes et al. 2001; Barnes 1998). Once the data are cubed, a further bandpass-removal algorithm, LUTHER (Barnes et al. 2001), is run on each of the cubes. This algorithm makes a polynomial fit to the continuum sources in a data cube then subtracts this template from each of the spectra in the gridded cube, which results in a cube for which the flux from continuum sources is minimized. The velocity resolution is 18 km s^{-1}, but the channel separation after cubing is 13.2 km s^{-1}. The rms noise level in the final cubes is ~13 mJy beam^{-1}. An example of the data quality can be seen in Figure 1. This figure shows a position-velocity diagram of part of a HIPASS cube. Galactic emission is seen at ~0 km s^{-1}, and the galaxy ESO 099-G005 is obvious at ~3600 km s^{-1}.

The region of sky cataloged for this paper was the SCC region of the sky, $\delta < -62^\circ$. This was one of the first regions of the sky to be completed to the full sensitivity of HIPASS. The SCC region comprises 45 HIPASS cubes, and represents ~11% of the HIPASS survey. The solid angle covered in the region is 0.74 steradians, and the total volume covered over the full velocity range is ~10^6 Mpc^3.

3. CATALOG

A catalog of H I–selected galaxies was compiled from the SCC region of the sky, $\delta < -62^\circ$. The catalog contains 536 galaxies, and 114 of these (21%) have no previous optical

[18] The Parkes telescope is part of the Australia Telescope, which is funded by the Commonwealth of Australia for operation as a National Facility managed by CSIRO.

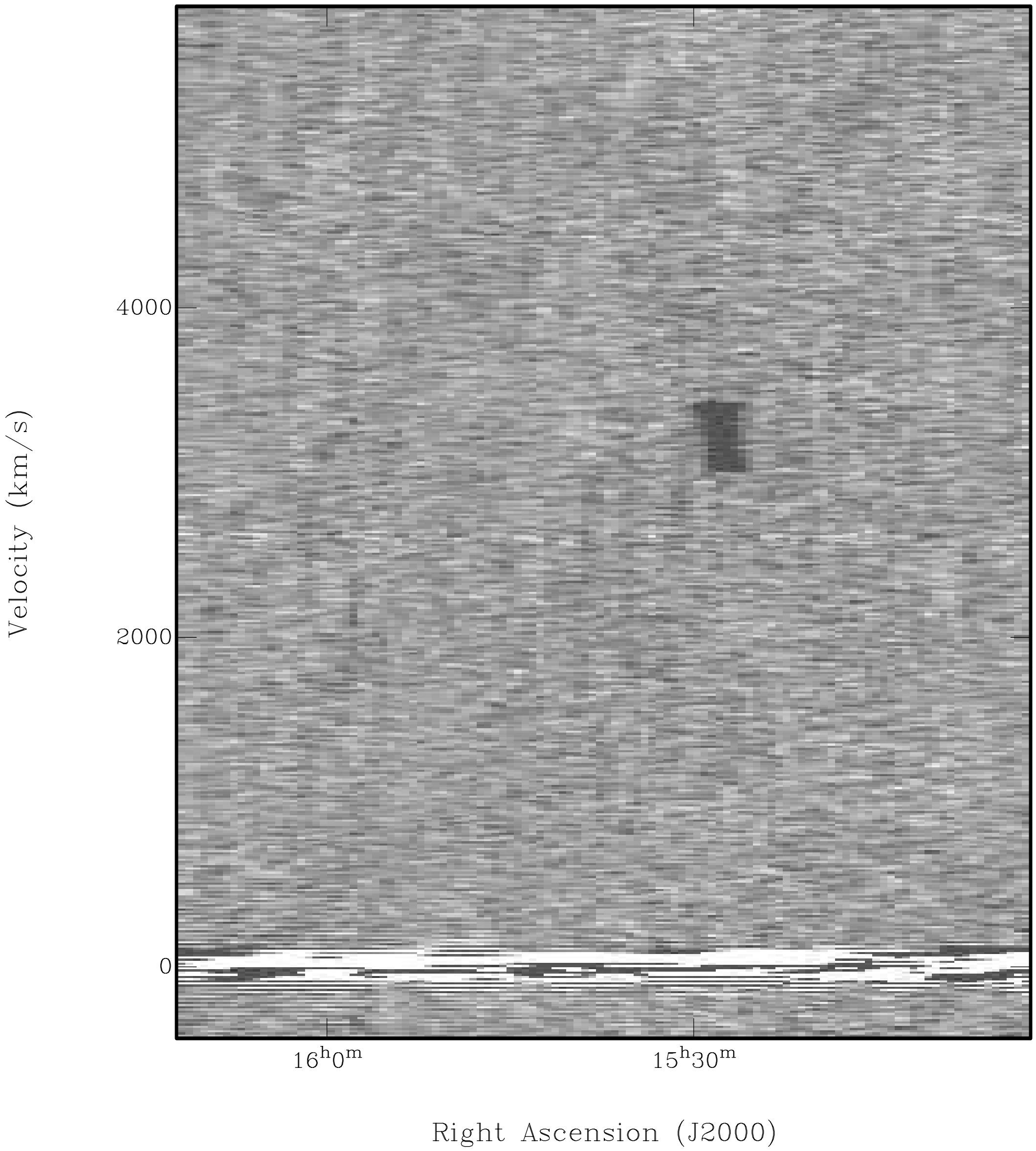

FIG. 1.—Section of a HIPASS data cube at roughly constant declination, $-64°11'58''.93$ (J2000.0). Visible are Galactic H I emission at 0 km s^{-1} and the galaxy ESO 099-G005 at ~3600 km s^{-1}.

identification. In addition, new redshifts were determined for 134 previously cataloged optical galaxies. All galaxies found in the SCC region have a positive radial velocity, even though the negative velocities were searched for galaxies.

Each candidate galaxy was checked in the NASA/IPAC Extragalactic Database[19] (NED) for a known optical counterpart. Optical images for all the galaxies were obtained from the First Generation Digital Sky Survey[20] (DSS I); for those with no optical counterpart in the First Generation Survey, the image from the Second Generation Digital Sky Survey (DSS II) was obtained. As the beam size of the survey is large, there is the possibility for confusion about the optical counterpart to an H I detection for which there is no available optical redshift. In the case for which an optical redshift was not available, the nearest cataloged optical galaxy is suggested as the counterpart to the H I detection. Optical redshifts, or H I synthesis observations, will be needed in the future to confirm these optical counterparts. A small number of new detections lie at low velocities in optically unobscured regions, yet do not have obvious optical counterparts in either of the DSS images. One of these detections, HIPASS J1712-64, has been studied in detail, but the nature and formation of this cloud is still uncertain (Kilborn et al. 2000). The nature of these new H I clouds will be discussed in a subsequent paper.

3.1. *Galaxy Selection*

The catalog was produced as follows. The candidate galaxy list was formed by visually searching the data cubes.

[19] The NASA/IPAC Extragalactic Database (NED) is operated by the Jet Propulsion Laboratory, California Institute of Technology, under contract with the National Aeronautics and Space Administration.

[20] The Digitized Sky Survey, provided by the Space Science Institute, based on photographic data from the UK Schmidt Telescope.

The visual display program KVIEW (Gooch 1995) was used to search through the data in three dimensions by displaying the data in two axes and stepping through the third. Bright galaxies with narrow line widths were most easily seen when the data cube was displayed in right ascension versus declination and stepped through velocity. Faint galaxies with large line widths were more easily discovered when the data cube was displayed as right ascension or declination versus velocity.

It was necessary to impose selection criteria when cataloging the galaxies to generate a consistent list of H I detections. The selection criteria for this visual sample were that a detection must (1) be easily visible above the local noise ($\sim 3\ \sigma$), (2) have spatial extent either greater than or equal to the beam size (to exclude interference), and (3) be visible over two or more velocity channels. Negative velocity regions were searched, but the heliocentric velocity range -100 km s^{-1} $\lesssim V \lesssim$ 200 km s^{-1} was not searched for galaxies because of confusion caused by Galactic H I emission. The Large and Small Magellanic Clouds and Magellanic Stream and Leading Arm were also excluded from the search region, in the following spatial and velocity ranges. The Large Magellanic Cloud lies at R.A. = 05^{h}23^{m}, decl. = $-69°45'$ (J2000.0), at a heliocentric velocity of 278 km s^{-1}. It has an H I line width of $\sim$150 km s^{-1} and a spatial extent of $\sim 15° \times 13°$. The Small Magellanic Cloud (SMC) lies at R.A. = 00^{h}52^{m}, decl. = $-72°49'$ (J2000.0), at a heliocentric velocity of 158 km s^{-1}. The SMC has an H I line width of $\sim$130 km s^{-1} and a spatial extent of $\sim 7° \times 4°$. The Magellanic Stream, Leading Arm, and associated emission are present in the SCC region, between a heliocentric velocity of about +80 and about +400 km s^{-1} (see Putman et al. 1998). Some regions obviously contained high-velocity clouds (HVCs; see Wakker & van Woerden 1991 for a review of HVC properties), consisting of a continuous distribution of resolved, narrow-width objects, with $V \lesssim 450$ km s^{-1}; these regions were not searched for galaxies because of the high probability of confusion (see Putman et al. 2002 for a catalog of HVCs in the region). Any detection that was found in the HVC velocity range but which was isolated and had no other HVCs in the same cube was cataloged as a possible galaxy. Therefore six of the detections included in the sample with low radial velocity have ambiguous identities as to their status as an HVC or galaxy. In addition it is likely that some nearby galaxies are not included in the catalog if their H I emission lies near that of the HVCs. Higher spatial and velocity resolution observations will be needed to distinguish such galaxies from Galactic and HVC H I emission.

To supplement the pure visual examination of the cubes, some objects were added to the catalog as a result of running automated galaxy-finding algorithms through the data. These finders, MultiFind by Kilborn (2001) and a wavelet-based finder by M. Howlett (2001, private communication), are in a preliminary state of readiness, but produced an additional set of objects, 41 of which were confirmed by visual examination and satisfied the same criteria as described above. Mostly these were faint objects with a peak flux $\lesssim 5\ \sigma$ or objects mistakenly missed in the visual search. Their inclusion increases the numbers of faint galaxies available for study, although as discussed later (§ 5 and Kilborn 2002), it does not make the present catalog complete at low flux density levels.

3.2. *Parameterization and Classification of the Galaxies*

For each of the detections, the parameters such as flux density, heliocentric velocity, and line width were measured in a semiautomated manner. A script was developed to step through the fitting process, accepting user input at each stage. Using a semiautomated script ensures that the measurements are consistent, yet the user input allowed for reality checks as the measurements were made. MIRIAD routines were used at each step in the fitting process.

First, a two-dimensional Gaussian fit (IMFIT) was made to a velocity-integrated map of each detection to determine the central position of the galaxy, as well as the spatial extent of the H I. The central position was then used to generate a spatially integrated spectrum of the detection, using a box size based on the extent of the H I. The spectrum was generated using MBSPECT, which gave a measurement of the peak and integrated flux of each detection, as well as the 50% and 20% velocity width, rms noise, and heliocentric velocity. The heliocentric velocity was measured as the central velocity at the 20% velocity width.

The Local Group correction for the radial velocities used in this paper is

$$V_{\rm LG} = V + 300 \sin l \cos b \ , \qquad (1)$$

where $V_{\rm LG}$ is the Local Group velocity, V is the heliocentric velocity in optical convention, and l and b are the Galactic longitude and latitude. At low velocities, especially $V < 500$ km s^{-1}, the distance that can be derived from these corrected velocities is only an estimate because of peculiar motions arising from gravitational interactions with other galaxies.

The galaxies in the SCC sample have been classified according to their optical morphology. The classification followed the scheme described in the Carnegie Atlas of Galaxies (Sandage & Bedke 1994). Classifications of previously cataloged optical galaxies were taken from the NED database. It is possible that incorrect or misleading classifications have been made with galaxies of small optical angular extent because of the poor resolution of the DSS I images. Thus the optical types have been divided into four broad classes for analysis: early types (E/S0), early spiral galaxies (Sa–b), late spiral galaxies (Sc–d), and late types (Sm, Im, Irr/pec, and dwarf), ignoring any bars. In addition, a number of galaxies could not be classified because of optical obscuration from the Galactic plane. The final problem for optical classification of galaxies was possible confusion in the Parkes beam. Galaxies were flagged if the optical counterpart was confused or interacting or if an optical identification was not possible. A galaxy was labeled as confused if there was more than one optical galaxy either of unknown redshift or with the same known redshift as the H I detection within a 5′ radius of the HIPASS position.

Table 1 is the SCC catalog of galaxies with derived H I fluxes, and optical properties if available. Column (1) lists the HIPASS name; column (2), right ascension (J2000.0); column (3), declination (J2000.0); column (4), heliocentric velocity, determined as the center of the 20% velocity width from MBSPECT (in kilometers per second); column (5), 20% velocity width (in kilometers per second); column (6), 50% velocity width (in kilometers per second); column (7), peak flux density (in janskys); column (8), total flux (in jansky kilometers per second); column (9), log $M_{\rm H\,I}$ in solar masses ($V_{\rm LG}$ corrected as in eq. [1]); column (10), previously

TABLE 1

South Celestial Cap H I Catalog

Name (1)	R.A. (J2000.0) (2)	Decl. (J2000.0) (3)	Vel (km s^{-1}) (4)	ΔV_{50} (km s^{-1}) (5)	ΔV_{50} (km s^{-1}) (6)	S_{peak} (Jy) (7)	S_{int} (Jy km s^{-1}) (8)	log $M_{H I}$ ($M_\odot$) (9)	Optical ID (10)	V_{opt} (km s^{-1}) (11)	Morphology (12)
HIPASSJ0002−80	00 02 54.1	−80 20 21.1	1959	130	97	0.218	20.53	9.43	ESO 012- G014	1953	SBm
HIPASSJ0014−70	00 14 01.2	−70 02 32.9	4190	105	78	0.120	8.15	9.76	ESO 050- G006	4135	SBcd
HIPASSJ0019−77	00 19 50.6	−77 06 12.7	1790	140	118	0.171	16.78	9.26	ESO-LV 0280141	...	SBb[a]
HIPASSJ0020−63	00 20 59.2	−63 52 35.9	1760	189	168	0.084	10.68	9.07	ESO 078- G022	1775	Sb
HIPASSJ0032−64	00 32 02.2	−64 18 52.5	2661	465	390	0.113	32.22	9.94	AM 0029-643	...	Sb[a]
HIPASSJ0039−76	00 39 39.6	−76 19 13.2	1758	99	69	0.053	3.49	8.56	...	...	dS0
HIPASSJ0040−63	00 40 54.0	−63 27 05.1	1713	194	157	0.174	24.92	9.41	ESO 079- G005	1721	SBcd
HIPASSJ0046−80	00 46 03.4	−80 46 43.9	4109	523	267	0.082	21.14	10.14	ESO 013-IG001	4169	Sa
HIPASSJ0049−66	00 49 57.4	−66 32 44.4	1666	142	113	0.057	5.33	8.71	ESO 079- G007	1674	Sa[b]
HIPASSJ0050−75	00 50 33.8	−75 19 40.5	4363	350	233	0.045	8.31	9.80	...	...	dI[b]
HIPASSJ0100−68	01 00 01.2	−68 09 14.5	6994	405	180	0.055	10.90	10.35	ESO 051- G011	6944	Sab
HIPASSJ0100−85	01 00 20.0	−85 32 31.5	4659	312	273	0.039	8.18	9.84	ESO 002- G012	4640	Sc
HIPASSJ0102−65	01 02 48.3	−65 37 44.8	2311	425	358	0.082	21.97	9.64	NGC 0360	2284	Scd
HIPASSJ0102−80	01 02 48.1	−80 13 58.4	1812	173	151	0.085	10.77	9.07	ESO 013- G009	1808	SBcd
HIPASSJ0107−69	01 07 27.0	−69 52 16.7	1506	266	242	0.197	39.64	9.47	NGC 0406	1509	SBc

Note.—Table 1 is presented in its entirety in the electronic edition of the Astronomical Journal. A portion is shown here for guidance regarding its form and content. Units of right ascension are hours, minutes, and seconds, and units of declination are degrees, arcminutes, and arcseconds.

[a] H I detections with a confused optical counterpart.

[b] Detections confirmed with Parkes narrowband observations.

cataloged optical name (if one exists); column (11), velocity of cataloged optical counterpart; and column (12), optical morphology. Galaxies that are confused in their identification are footnoted "a" on their optical classification. Detections that have been confirmed with further observations are footnoted "b" (see § 5 for details).

4. ACCURACY OF THE DERIVED HIPASS PARAMETERS

The accuracy of the HIPASS parameter values has been tested using two methods. First, high-resolution synthesis observations are compared with the HIPASS derived values, then the HIPASS derived fluxes are compared with those of published catalogs.

Follow-up H I synthesis observations were made at the Australia Telescope Compact Array[21] (ATCA). Thirty-seven candidates were observed with the ATCA, using either the 750 or 375 m arrays, of which 27 galaxies were detected. Galaxies without previous optical identifications or without obvious optical counterparts were chosen for these observations. The observations were made using an 8 MHz bandpass with 512 channels, which gave a channel separation of 3.3 km s^{-1}, and with an FWHM resolution of 4.0 km s^{-1} before smoothing. The observations were made in "snapshot" mode, with typically 5 or 6 cuts, giving total integration time of ~3 hr. The data were reduced using the MIRIAD data reduction package. A secondary calibrator was observed with each galaxy to calibrate the phase, and the primary calibrator, PKS 1934−638, was used to set the primary flux density scale. The data were edited and calibrated, and the bandpass was removed. Bright continuum sources were removed by fitting and subtracting straight lines to the line-free channels in the visibility domain, using the MIRIAD task UVLIN. The data were then cubed using natural weighting to give the source the highest signal-to-noise ratio possible. The cubes were CLEANed until the absolute maximum residual fell below 3 times the theoretical noise for the cube (typical rms ~7 mJy $beam^{-1}$). Finally, the data were RESTORed and Hanning-smoothed.

Table 2 gives the H I derived parameters for the galaxies from the ATCA follow-up observations. Column (1) lists the HIPASS name; columns (2) and (3), central right ascension and declination (J2000.0) from the ATCA data; column (4), heliocentric velocity (in kilometers per second); columns (5) and (6), 50% and 20% velocity width, derived from the MIRIAD task MBSPECT (in kilometers per second); column (7), peak flux density, derived from the spatially integrated Hanning-smoothed spectrum, using MBSPECT (in janskys); column (8), integrated flux, also derived from MBSPECT (in jansky kilometer per second); column (9), observation month and year; and column (10), ATCA array used for the observations.

Ten candidates were not detected in the ATCA observations. Three of the detections had low peak flux densities (<3 σ). In Parkes confirmation follow-up observations (see § 5), two of these low-flux sources were not redetected and

[21] The Australia Telescope Compact Array is funded by the Commonwealth of Australia for operation as a National Facility managed by CSIRO.

TABLE 2
DERIVED PARAMETERS FOR THE 27 GALAXIES DETECTED WITH ATCA

HIPASS Name (1)	R.A. (J2000.0) (2)	Decl. (J2000.0) (3)	Vel. (4)	ΔV_{20} (km s^{-1}) (5)	ΔV_{50} (km s^{-1}) (6)	S_{peak} (Jy) (7)	S_{int} (Jy km s^{-1}) (8)	Obs. (9)	Array (10)
HIPASSJ0039-76......	00 39 08	−76 20 12	1739	92	56	0.076	3.1	1999 Jun	750
HIPASSJ0116-63......	01 16 48	−63 30 01	2301	136	119	0.017	1.3	1999 Jun	750
HIPASSJ0159-83......	02 00 11	−83 59 16	3498	109	93	0.045	3.0	1998 Dec	750
HIPASSJ0209-75......	02 09 01	−75 56 11	1653	188	175	0.048	5.14	1997 Oct	375
HIPASSJ0305-69......	03 05 24	−68 56 31	1364	131	117	0.033	2.4	2000 May	750
HIPASSJ0411-70......	04 11 38	−70 14 13	7155	79	65	0.030	1.1	2000 May	750
HIPASSJ0511-72......	05 11 34	−72 18 21	1525	92	72	0.064	3.8	1997 Oct	375
HIPASSJ0554-71......	05 54 42	−71 55 50	1473	64	58	0.044	2.2	1997 Oct	375
HIPASSJ0729-75......	07 28 43	−75 03 21	1118	136	80	0.092	6.3	1999 Jun	750
HIPASSJ0751-62......	07 51 33	−62 19 59	6106	77	56	0.024	1.3	1999 Dec	375, 750
HIPASSJ0908-64......	09 08 21	−64 42 10	1839	73	39	0.073	3.4	1999 Jun	750
HIPASSJ1004-73......	10 05 03	−73 51 15	1243	58	42	0.152	5.7	1998 Jun	750
HIPASSJ1150-69......	11 51 35	−69 48 26	6810	73	26	0.035	1.2	2000 May	750
HIPASSJ1242-77......	12 42 06	−77 55 19	2654	76	64	0.057	2.9	1998 Jun	750
HIPASSJ1247-77......	12 47 35	−77 34 53	413	50	29	0.122	4.1	1998 Jun	750
HIPASSJ1339-72......	13 39 23	−72 54 54	3220	149	136	0.032	2.4	1998 Jun	750
HIPASSJ1407-75......	14 07 28	−75 53 24	2795	145	108	0.089	8.0	1998 Jun	750
HIPASSJ1456-72......	14 56 42	−72 33 10	3110	154	121	0.041	3.2	2000 May	750
HIPASSJ1512-72......	15 11 56	−72 51 28	3000	424	408	0.211	61.1	2000 May	750
HIPASSJ1648-69......	16 48 13	−69 08 14	4683	352	313	0.105	16.1	1999 Jun	750
HIPASSJ1650-62......	16 49 49	−62 33 05	4226	122	89	0.042	2.7	2000 May	750
HIPASSJ1705-68......	17 05 55	−68 57 33	7826	348	288	0.021	3.5	1999 Dec	750
HIPASSJ1816-67......	18 15 45	−67 01 36	3312	190	183	0.058	7.0	1999 Jun	750
HIPASSJ2039-63......	20 39 01	−63 46 15	1644	65	52	0.091	4.1	1999 Dec	750
HIPASSJ2214-67......	22 13 46	−67 24 19	3178	56	41	0.036	1.2	1999 Jun	750
HIPASSJ2247-73......	22 48 14	−73 48 49	3378	167	154	0.013	1.3	1997 Oct	375
HIPASSJ2309-74......	23 08 40	−74 49 52	2073	147	98	0.019	1.4	1998 Jun	750

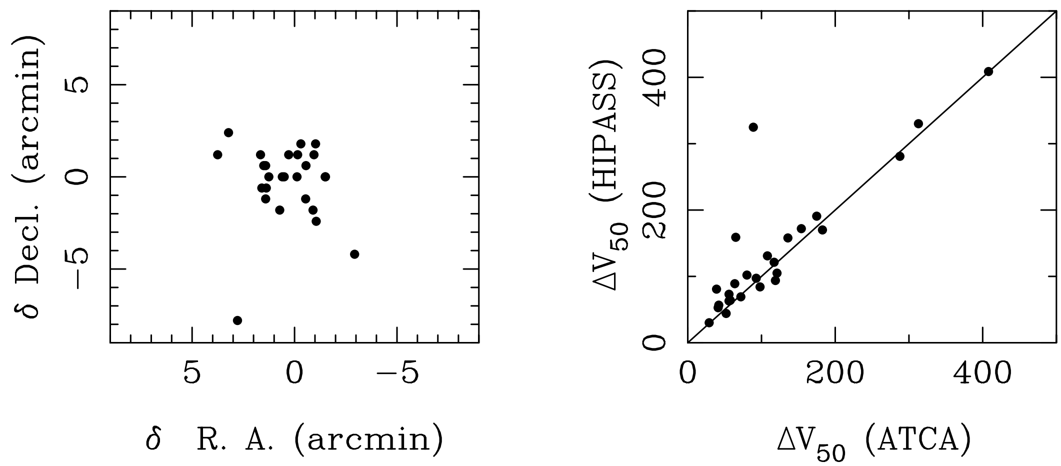

FIG. 2.—*Left*: Difference in right ascension and declination for the ATCA measurements and HIPASS measurements. The rms of the scatter is 2′.1 for right ascension and 1′.7 for declination. *Right*: ΔV_{50} from HIPASS vs. ΔV_{50} from the ATCA. The solid line represents equal velocity width measurements. Two measurements lie far away from this line because of the ATCA resolving out part of the flux of these galaxies.

thus were taken out of the sample and one was redetected and therefore kept in the sample. The remaining seven candidates lay well above the HIPASS noise but were resolved out in the ATCA data (all were observed using the 750 m array).

The positional accuracy of the original HIPASS detections is now compared with the follow-up ATCA observations. Figure 2 (*left*) shows the difference in position between the ATCA and HIPASS observations. No correlated offset can be seen between the two sets of H I positions, and the rms of the scatter for the offset is 1′.9 including both right ascension and declination. This compares with the predicted range of positional errors from the gridding process of $\sim 3'$ for a 3 σ detection to $\sim 1'$ for a 10 σ detection (Barnes 1998). The object with the largest ATCA-to-HIPASS offset (HIPASS J0305-69) is lying on an interference spike in the original HIPASS cube, which hampered the calculation of its centroid position.

Figure 2 (*right*) shows the ATCA and HIPASS measurements for the 50% velocity width. The two measurements agree well for most of the sample. There are two galaxies for which the velocity width determined from HIPASS is higher than the ATCA-derived velocity width. HIPASS J1650-62 has a low signal-to-noise ratio, and the difference in measurements appears to be due to noise in the spectrum. The flux detected in the ATCA observations is just 22% of the flux detected in HIPASS, and this appears to have affected the velocity measurement of this galaxy as well. The higher velocity emission was not detected in the ATCA data, leading to the conclusion that the higher velocity channels of this galaxy contain extended emission. HIPASS J0908-64 also has a substantial difference between the HIPASS-derived ΔV_{50} and the ATCA ΔV_{50}. This galaxy is a strong source, but the ATCA map indicates some extended emission, and the lower flux emission may have been missed in the ATCA spectrum. In fact, 70% of the HIPASS flux is missed in the ATCA observations. Most of the galaxies had a lower total flux measure from the ATCA observations, as expected because of the incomplete UV coverage in the synthesis observations. However, the full flux was detected for seven of the 27 galaxies. The velocities determined from the ATCA and HIPASS observations matched very well, apart from HIPASS J1650-62, which was previously discussed.

In addition to the synthesis observations, two catalogs have been used to compare and check the fluxes derived from HIPASS. Huchtmeier & Richter (1989) compiled a catalog of 9500 galaxies. Forty-one galaxies in the SCC sample had entries for total integrated flux in this catalog. The second comparison catalog was compiled by Mathewson, Ford, & Buchhorn (1992), who published H I data from pointed observations of 551 galaxies observed with the Parkes Telescope. Thirty-three galaxies from this catalog were present in the SCC sample. Figure 3 shows a comparison of integrated flux for the overlapping 74 galaxies from both catalogs. The fluxes from the homogeneous Mathewson et al. (1992) catalog agree very well with the HIPASS derived fluxes, while the heterogeneous Huchtmeier &

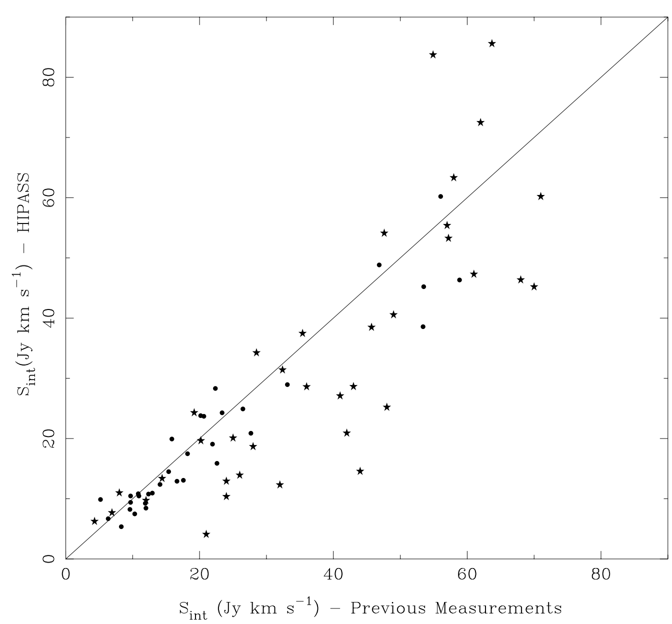

FIG. 3.—Integrated flux measurements from the Huchtmeier & Richter (1989) catalog (*stars*) and the Mathewson, Ford, & Buchhorn (1992) catalog (*circles*), compared with HIPASS measurements. The Mathewson et al. (1992) measurements compare quite well with HIPASS fluxes, while the Huchtmeier & Richter (1989) measurements tend to be higher. The HIPASS fluxes tend to be lower than the previous measurements.

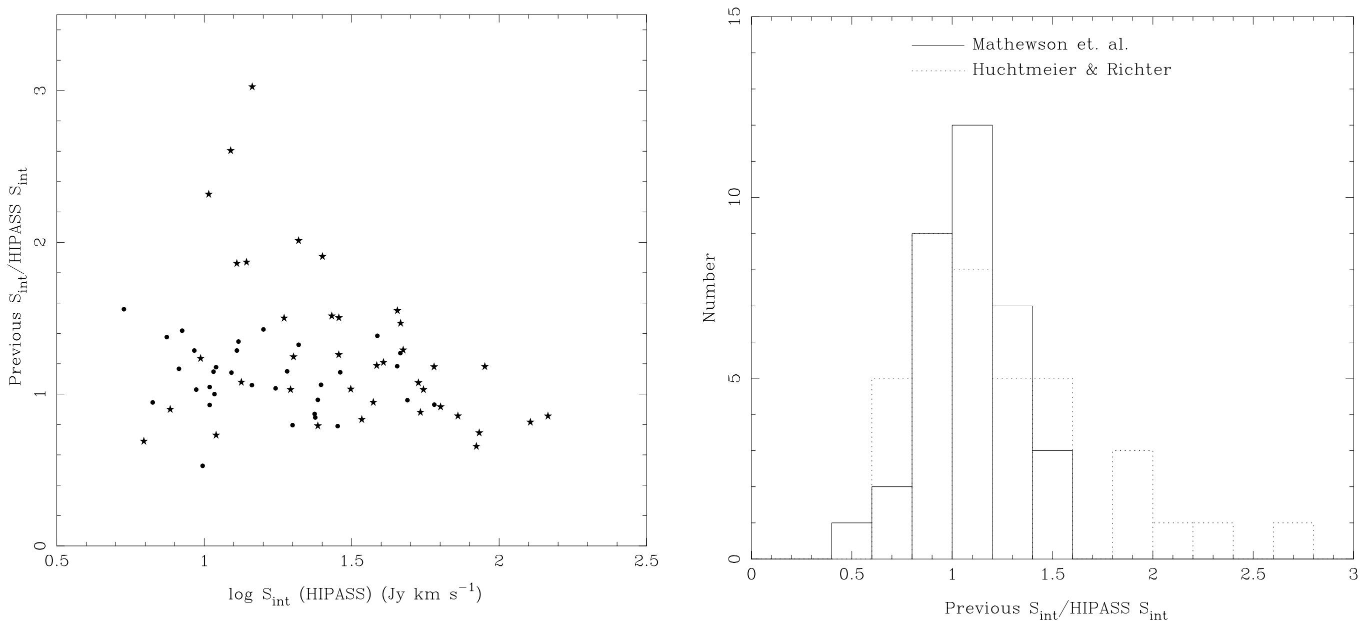

FIG. 4.—*Left*: No relationship is seen between the ratio of previous to HIPASS fluxes with integrated flux. The symbols are the same as in Fig. 3. *Right*: The corresponding histogram of flux ratios. Most of the Mathewson et al. (1992) fluxes agree with the HIPASS fluxes within 20%. The scatter is larger for the Huchtmeier & Richter (1989) fluxes.

Richter (1989) fluxes agree to a lesser extent. There is no dependence on the flux ratio with the flux of the galaxies (see Fig. 4). The fluxes agree to ~20% for the Mathewson et al. (1992) comparison and significantly worse for the Huchtmeier & Richter (1989) compilation.

5. COMPLETENESS AND RELIABILITY

Well above the flux density limit, the SCC catalog is expected to be complete and reliable. However, closer to the flux density limit this situation changes. The approximate 3 σ flux density detection limit for the catalog is 39 mJy beam^{-1}; however, due to variations in the rms level for the different cubes, and as the sources were selected largely by visual inspection, the initial catalog contained sources with peak flux densities down to 20 mJy. Figure 5 shows the rms of each of the cubes in the SCC region, calculated using the AIPS++ STATS routine. This shows that while the mean rms is ~13 mJy beam^{-1}, the actual rms of each cube varies from 9 to 17 mJy beam^{-1}, depending on the cube. This means that galaxies in particular cubes are more detectable than others. The main variation arises where the cubes cross the Galactic plane, as at this position the occurrence of recombination lines is higher and the number of continuum sources is higher in these regions. Because of this rms variation, a large number of galaxies were cataloged with a peak flux density of less than the average 3 σ value of 39 mJy.

To test the reliability of the catalog, a selection of sources were reobserved at the Parkes radiotelescope, using the narrowband receiver in pointed mode. The sources had a variety of peak flux densities, ranging from 20 mJy to over 200 mJy. From these confirmation tests it was found that the reliability of detections with a peak flux density less than the mean 3 σ (39 mJy) was poor. Only 50% of the galaxies observed at these low flux densities were redetected. However, above the 3 σ limit, the redetection rate was extremely good. Only one galaxy with a peak flux density of 41 mJy was not redetected. Because of this, all sources with a peak flux density less than 39 mJy and a number of other sources with a range of peak flux densities were subsequently reobserved in narrowband mode at Parkes. About 50% of the candidates were redetected, and those that were not were taken out of the catalog. The catalog presented in this paper is now expected to contain few false detections; thus the reliability is very high. Figure 6 shows a plot of velocity width versus peak flux density for the sources that were confirmed at Parkes (*circles*), those not confirmed (*crosses*), and those

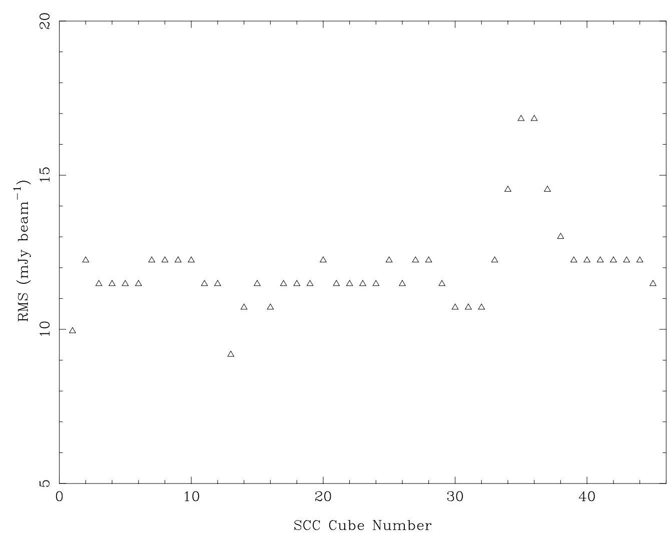

FIG. 5.—Plot of rms noise in SCC cubes. The rms is higher in cubes that lie near the Galactic plane. HIPASS cubes are approximately 8° × 8°. Cube 1 is centered at decl. −90°; cubes 2–9 are centered between right ascension 0^h and 24^h at decl. −82°; cubes 10–24 are centered between right ascension 0^h and 24^h at decl. −74°, and cubes 25–45 are centered between right ascension 0^h and 24^h at decl. −66°. The quantization of the rms values is caused by the 16-bit integer precision used in the cubing.

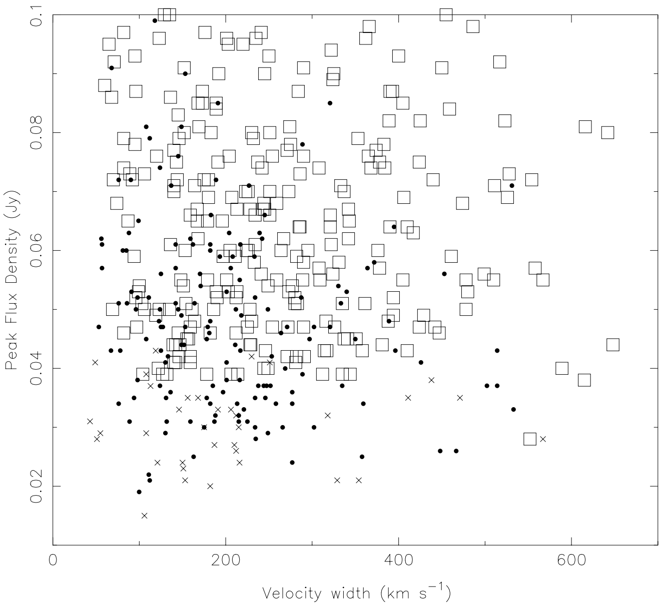

FIG. 6.—Narrowband confirmation detections, showing galaxies yet to be confirmed (*squares*), confirmed detections (*circles*), and galaxies not reconfirmed in pointed narrowband observations (*crosses*). Galaxies with lower flux densities tended to be less reliable, and the velocity width of the detection does not seem to correlate with the reliability.

yet to be observed (*squares*). It can be seen that all galaxies reobserved with a peak flux density above 41 mJy were redetected, and there does not seem to be any relationship between the reliability of a detection and its velocity width.

Even though the reliability of this catalog is high, near the flux density limit, the catalog is incomplete, meaning that it is most likely missing many weak sources. The completeness of the catalog is difficult to define particularly as sources were selected largely by visual inspection. Therefore, for statistical purposes, further flux density cuts will be required. Appropriate values for mass function calculation are discussed by Kilborn (2002).

6. CHARACTERISTICS OF THE SAMPLE

The characteristics of the sample are summarized in Table 3. Galaxies were detected from 300 to 10,610 km s^{-1}. Below a velocity of 2000 km s^{-1} the number of galaxies detected by HIPASS outnumbers that with already known redshifts from optical surveys. One hundred fifty-five galaxies were detected with a velocity less than 2000 km s^{-1} in HIPASS, compared with the 112 optically identified galaxies that have known redshifts from the NED database. Of the 112 already known galaxies with redshifts, 82 were redetected with HIPASS. Thus the total number of galaxies with known redshifts less than 2000 km s^{-1} in the SCC region is now 185. The velocity distribution of galaxies in the south celestial cap compared with that of all NED galaxies[22] of known velocity in the same region is shown in Figure 7. It is evident that the velocity distribution of HIPASS galaxies does not follow that of optical galaxies in NED. This is expected as the sensitivity limits for optical surveys and

TABLE 3
CHARACTERISTICS OF THE SCC SAMPLE

Parameter	Value
Area surveyed (deg^2)	2400
Velocities surveyed (km s^{-1})	−1200–12,700
Velocities cataloged (km s^{-1})	300–10,610
Average rms (mJy beam^{-1})	13
Number of galaxies in catalog	536
New galaxies	114
New redshifts (of cataloged galaxies)	134
Mass range ($M_\odot$)	5×10^6–9×10^{10}
Mean velocity (km s^{-1})	3313
Mean ΔV_{20} (km s^{-1})	240
Mean ΔV_{50} (km s^{-1})	186
Mean $M_{\rm H\,I}/L_B$ ($M_\odot/L_\odot$)	1.7

HIPASS are different. In addition, HIPASS may not detect nearby clusters of galaxies because of their deficiency in neutral gas. Solanes et al. (2001) find that $\frac{2}{3}$ of the clusters they surveyed showed a deficiency of H I near the core, which suggests that HIPASS may tend to miss such clusters. So while many optical surveys concentrate on optical clusters, HIPASS may not detect them at all. This effect was most recently seen by Waugh et al. (2002), who looked at HIPASS data of the Fornax Cluster and found very few galaxies in the central regions of the cluster. The large beam size of the Parkes telescope also makes the individual detection of galaxies in clusters harder, with the problem rising with increasing distance to the cluster.

The H I mass distribution for the SCC sample is shown in Figure 8*a*. The dashed line represents the distribution for the whole sample, and the solid line shows the H I mass distribution of newly detected galaxies. The mass range for the sample is larger than for previous surveys, with the lowest-mass galaxy having $\sim 5 \times 10^6$ $M_\odot$ of H I and the highest-mass galaxy, $\sim 9 \times 10^{10}$ $M_\odot$ of H I. Most of the H I mass in the sample is contained in galaxies with $M_{\rm H\,I} \sim$

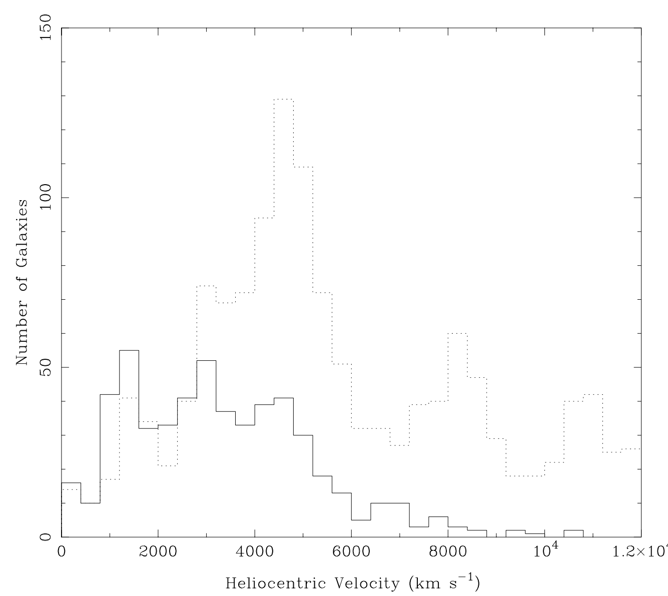

FIG. 7.—Velocity distribution of the SCC sample (*solid line*) and all galaxies in the NED database with known redshift (*dotted line*).

[22] It is noted that the NED optical catalog is heterogeneous, so that comparison is difficult.

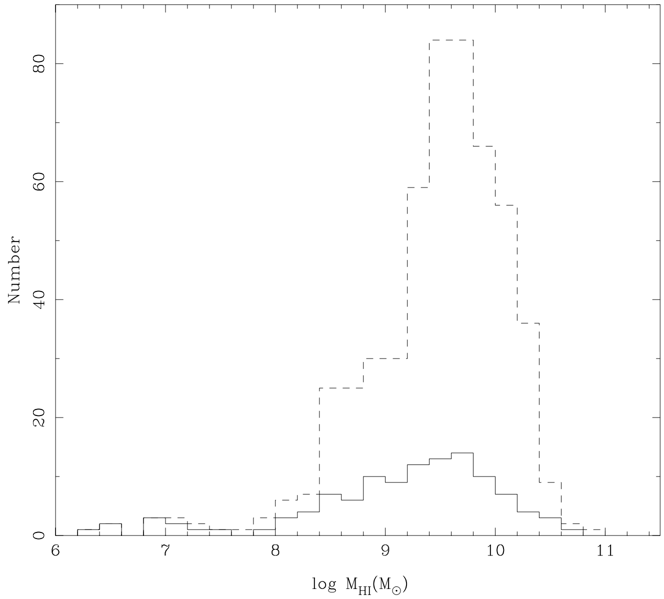

FIG. 8*a*

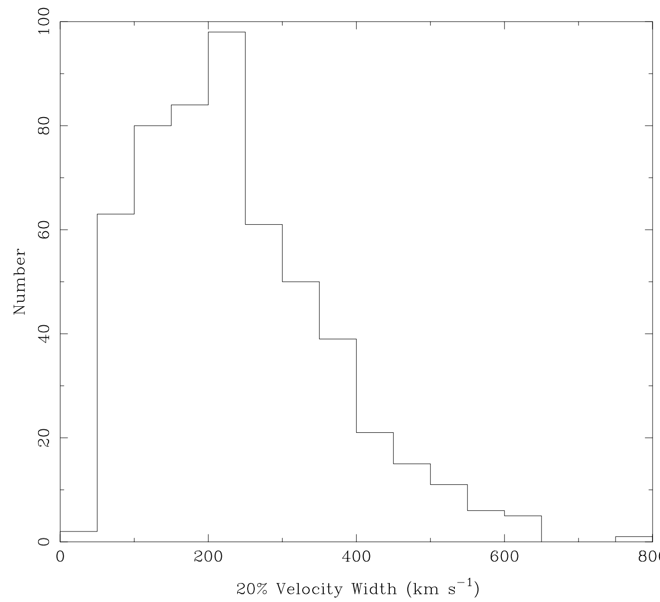

FIG. 8*b*

FIG. 8.—(*a*) H I mass distribution for the SCC sample, showing the H I mass distribution for the full sample (*dashed line*) and the H I mass distribution of the newly detected galaxies (*solid line*). (*b*) Distribution of 20% velocity widths for the SCC sample (not corrected for inclination).

10^9–10^{10} $M_\odot$. The highest-mass galaxy detected in the sample is HIPASS J2123-69, with a velocity of 10,247 km s^{-1}. There are several optical galaxies visible near the position of this H I detection, so higher resolution H I observations are needed to determine whether the high mass is due to confusion of two galaxies in the Parkes beam. Of the 10 most massive galaxies in the sample, only one lies closer than 6500 km s^{-1}, and that galaxy is NGC 6744, which lies at a velocity of $V_{LG} = 715$ km s^{-1}. Synthesis observations of all the most massive galaxies are currently underway at ATCA to determine whether these galaxies are single gravitationally bound objects or several galaxies confused in the Parkes beam. Overall, the H I mass distribution of the new galaxies follows that of the previously cataloged galaxies, although only new galaxies are present in the extreme H I mass bins.

Figure 8*b* shows the distribution of 20% velocity widths (ΔV_{20}) for the sample. The largest velocity width is $\Delta V_{20} = 770$ km s^{-1}, but this is a confused detection in the Parkes beam comprising the galaxies NGC 6872 and IC 4970. The smallest–velocity width galaxy in the sample is HIPASS J1614-72, which has $\Delta V_{20} = 35$ km s^{-1}, which is just twice the velocity resolution of HIPASS. This detection is one of the confused HVC/dwarf galaxies and lies at a low systemic velocity. The mean ΔV_{20} for the sample is $\Delta V_{20} = 240$ km s^{-1}, and the mean 50% velocity width for the sample is $\Delta V_{50} = 186$ km s^{-1}.

6.1. *Optical Properties*

The majority of galaxies in the SCC sample are classified as spirals (309 galaxies, or 68%). There were more late-type spirals than early, with 28% being Sa/Sb and 40% classified as Sc/Sd. The number of S0s in the sample is low, 20% or ∼6%, and there were just two galaxies classified as elliptical. The majority of the newly detected galaxies that could be optically identified were faint late types. Eighty-eight galaxies could not be optically identified either because of their Galactic obscuration or because of the presence of two or more possible optical candidates. Three galaxies were seen from their optical images to be interacting, and 68 galaxies were confused in the Parkes beam.

According to the NED database, 1398 galaxies with known redshifts have been cataloged optically in the SCC region. Of these, 793 have morphological classifications from NED. Four hundred forty-eight galaxies in the SCC catalog were able to be morphologically classified. The percentage breakdown of optical morphology of all optical galaxies in the SCC region with classifications compared with the breakup of optical types of the HIPASS galaxies is shown in Figure 9. The distribution of galaxy type in the optical catalogs is quite different from that in the HIPASS catalog. The optical catalogs contain a much higher per-

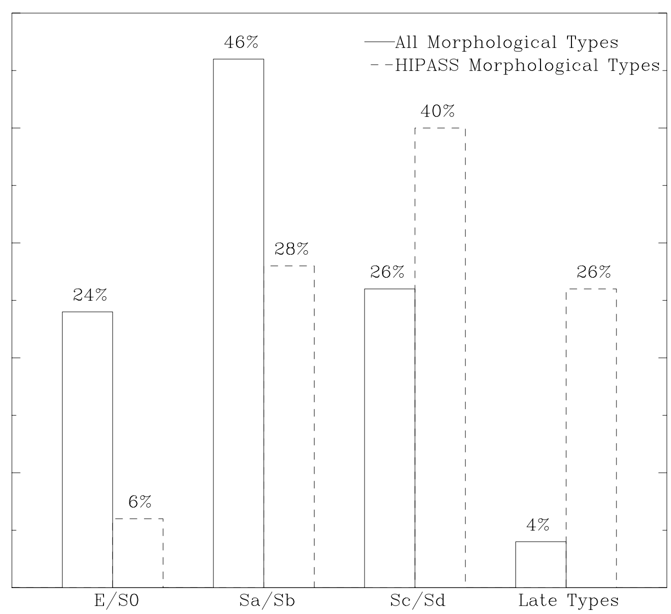

FIG. 9.—Morphological classifications for all optically identified galaxies in the SCC region (*solid line*) and all HIPASS galaxies in the SCC region (*dashed line*).

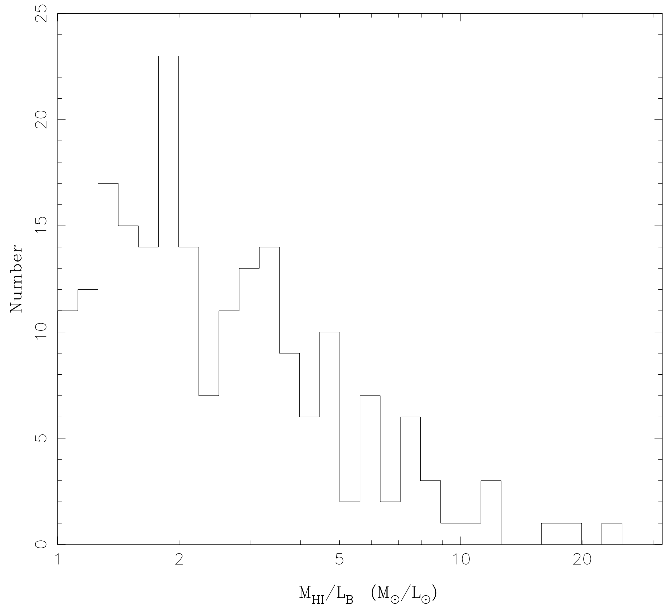

FIG. 10.—Distribution of H I mass-to-light ratios for galaxies with published ESO LV B magnitudes.

centage of early-type galaxies (24% optical compared with 6% HIPASS), while the HIPASS catalog has a much greater number of late-type galaxies (26% HIPASS compared with 4% optical). The percentage of spiral galaxies in each sample is similar, but the early spirals dominate the optical sample, while the late spirals dominate the HIPASS catalog.

Figure 10 shows the distribution of H I mass-to-light ratios for the SCC sample. The optical luminosity was determined from the B magnitudes given in the ESO LV catalog for the previously cataloged galaxies or from optical observations from the MSSSO 40 inch telescope (Marquarding 2000) for some of the new HIPASS detections. Most of the galaxies detected with HIPASS have an $M_{\rm H\,I}/L_B < 5$, but 28 galaxies have a higher $M_{\rm H\,I}/L_B$. The galaxy with the highest $M_{\rm H\,I}/L_B$ is HIPASS J0019-77, with $M_{\rm H\,I}/L_B = 24$. This is a previously known ESO galaxy, but the HIPASS observation represents the first H I detection. This particular detection may be confused, however, as there are two optical galaxies close by, and only one has a measured redshift. Table 4 gives the $\langle M_{\rm H\,I}/L_B \rangle$ for the different optical morphologies. The mean H I mass-to-light ratios for galaxies of different Hubble type varies from 1.8 for early types to 3.2 for late types. The average value for the early types in particular is quite high. Within the sample of 10 early types for which optical information was available, there is only one galaxy with an elliptical classification ($M_{\rm H\,I}/L_B = 0.3$), with the rest classified as S0 ($\langle M_{\rm H\,I}/L_B \rangle = 1.9$). Half the S0 galaxies are actually classified as S0 peculiar, possibly indicating an interaction in the past, and this could explain the high value for $\langle M_{\rm H\,I}/L_B \rangle$. Also two of the S0 galaxies are labeled as confused, and the H I may be associated with nearby Sc galaxies. The early and late spiral galaxies have similar $\langle M_{\rm H\,I}/L_B \rangle$, but the average value for the early spiral galaxies is influenced by the inclusion of HIPASS J0019-77, which has an $M_{\rm H\,I}/L_B$ of 24, which is much higher than the other early spiral galaxies. The median values show an increase in $M_{\rm H\,I}/L_B$ from early to late spiral galaxies.

TABLE 4
CHARACTERISTICS OF GALAXIES OF DIFFERENT OPTICAL CLASSIFICATION

Parameter	Early Type	Early Spiral	Late Spiral	Late Type
$\langle M_{\rm H\,I}/L_B \rangle$	1.8	2.0	2.2	3.2
Median $M_{\rm H\,I}/L_B$	1.3	1.3	1.6	2.1
Number with measured L_B	8	63	118	54

7. SPATIAL DISTRIBUTION OF THE H I–SELECTED GALAXIES

The distribution of the HIPASS galaxies on the sky is similar to the distribution of already known galaxies in the region. Figure 11 shows the HIPASS galaxies plotted with the previously cataloged galaxies with a redshift in the HIPASS detection range. The newly discovered HIPASS galaxies do not fill the voids, and they follow the general distribution of the optically cataloged galaxies. The exception is near the Galactic plane, where the catalog of optical galaxies is incomplete. Several optical clusters can be seen in Figure 11, e.g., the PAVO II cluster at $(l, b) = (332.3, -23.5)$ with $V = 4167$ km s^{-1}. This cluster has more than 30 optically classified members, yet only one is detected in HIPASS. The clustering properties and correlation function for this sample are investigated further in Tantisrisuk et al. (2002).

The distribution of HIPASS galaxies for different velocity ranges is now compared with known optical large-scale structure, based on maps by Fairall (1998). Figures 12 and 13 show the distribution of HIPASS galaxies: those with previous optical counterparts are indicated by filled circles, and galaxies with no previous optical identifications are shown with stars. The Magellanic Clouds are shown by the open circles on each plot. Major features are noted and are described below.

The main structure seen at the lowest velocities ($V < 1000$ km s^{-1}) is the edge of the Centaurus wall, which runs perpendicular to the Galactic plane at a Galactic longitude of $\sim 330°$. A number of new detections were discovered in this region. Mostly they are ambiguous HVC or galaxy detections without visible optical counterparts. The Centaurus

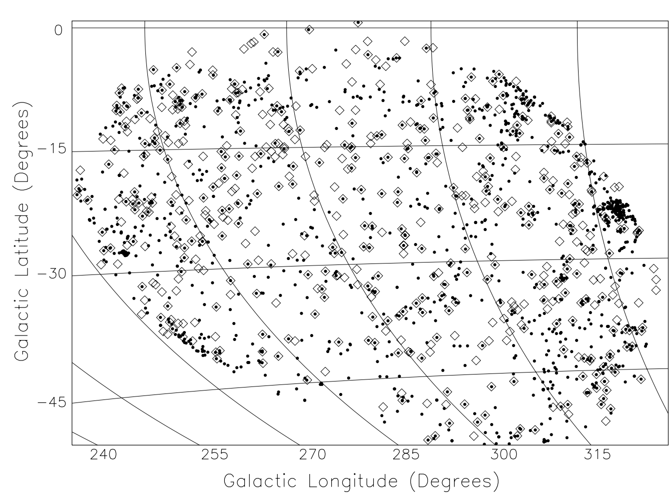

FIG. 11.—Spatial distribution of SCC galaxies, showing HIPASS galaxies (*diamonds*) and previously cataloged optical galaxies in the same velocity range as the SCC sample (*circles*).

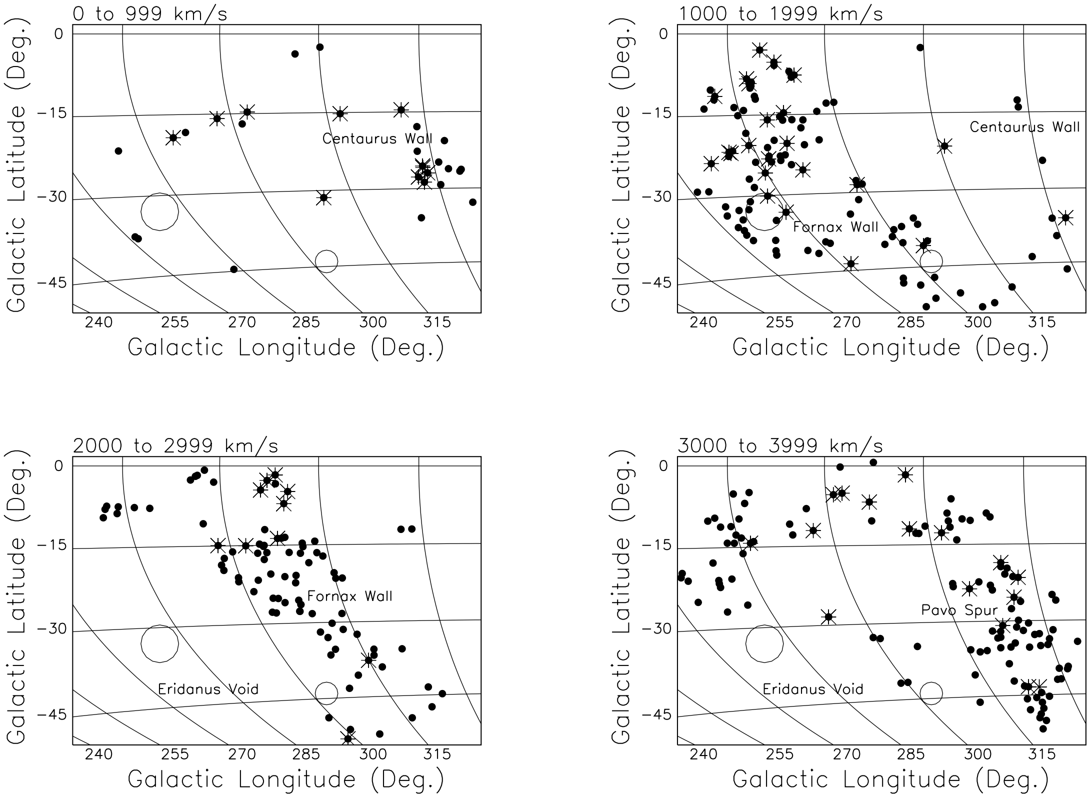

FIG. 12.—Distribution of south celestial cap galaxies in four velocity ranges, showing HIPASS detections with a known optical counterpart (*filled circles*), new HIPASS detections (*stars*), and the Magellanic Clouds (*open circles*).

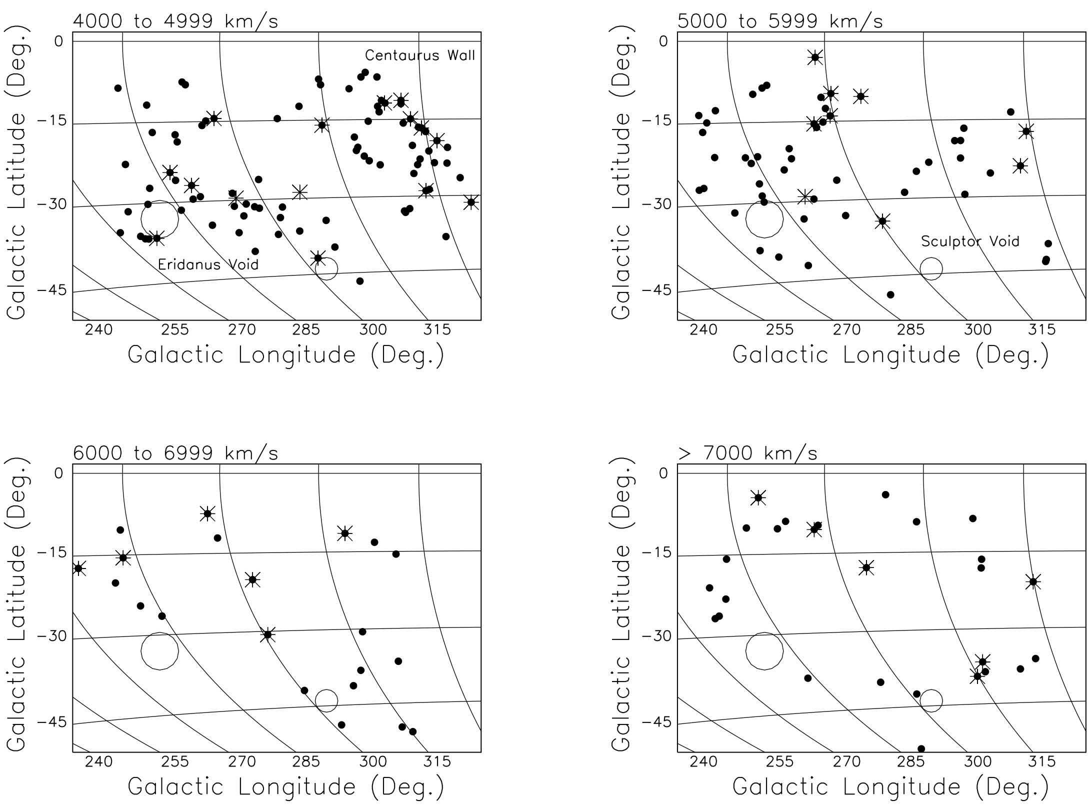

FIG. 13.—Same as Fig. 12, for four additional velocity ranges

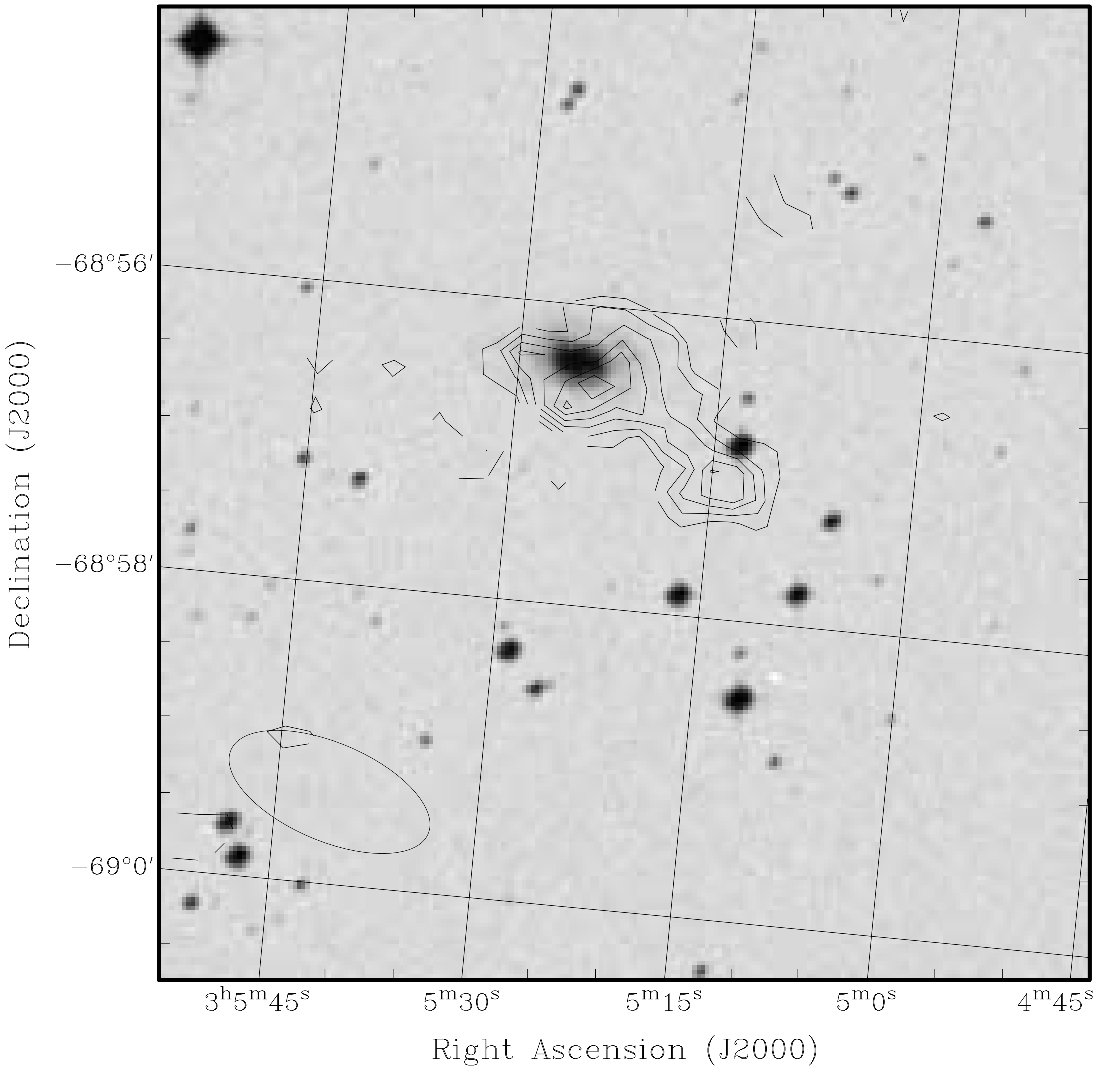

Fig. 14*a*

Fig. 14.—ATCA observations of previously uncataloged high surface brightness galaxies. The ATCA H I contours are overlaid on DSS I images. The optical counterparts are compact, resulting in their being missed in optical surveys. The beam for the H I observations is shown at the bottom left in each image. (*a*) HIPASS J0305-69. (*b*) HIPASS J1816-67.

wall is an edge-on feature that runs parallel to the Supergalactic plane. This velocity range represents only ~0.05% of the total volume of the SCC region, but this is the limiting velocity range for finding low-mass galaxies ($M_{\rm H\,I} \lesssim 10^8$ $M_\odot$).

Between velocities 1000 km s^{-1} and 1999 km s^{-1}, the Fornax wall appears: The Fornax Cluster lies off the plot in the direction of the upper right corner. The Fornax wall is a face-on feature. In the next velocity region (2000 to 2999 km s^{-1}) a fragment of the Fornax wall is present, and the Eridanus void can be seen in the bottom left of the plot. The structure of galaxies continues moving to the right as we look deeper in velocity, and between velocities of 3000 and 3999 km s^{-1} the Pavo spur is quite obvious and the Eridanus void is still present. There are a number of new galaxies toward the plane of the Galaxy at this velocity, and it is possible we are seeing a new structure that joins the Fornax and Centaurus clusters via the Fornax wall.

The edge of the Centaurus wall is evident again between the velocities of 4000 and 4999 km s^{-1}, and the Eridanus void is starting to disappear. The next velocity range, 5000 to 5999 km s^{-1}, contains the start of the Sculptor void, along with a several new galaxies toward the plane of the Milky Way.

Because of the sparsity of HIPASS detections above a velocity of 6000 km s^{-1}, no large-scale structure has been indicated. In the velocity range 6000 to 7000 km s^{-1}, new HIPASS galaxies outnumber HIPASS-detected galaxies with known optical counterparts. Once again the new galaxies tend to be found toward the plane of the Galaxy. There are still a significant number of new galaxies being detected above a velocity of 7000 km s^{-1}, and in this velocity range only large H I mass galaxies have flux limits above the HIPASS sensitivity limit.

8. PROPERTIES OF THE NEWLY DETECTED GALAXIES

One hundred and fourteen galaxies without previous NED identifications were found in the SCC region of

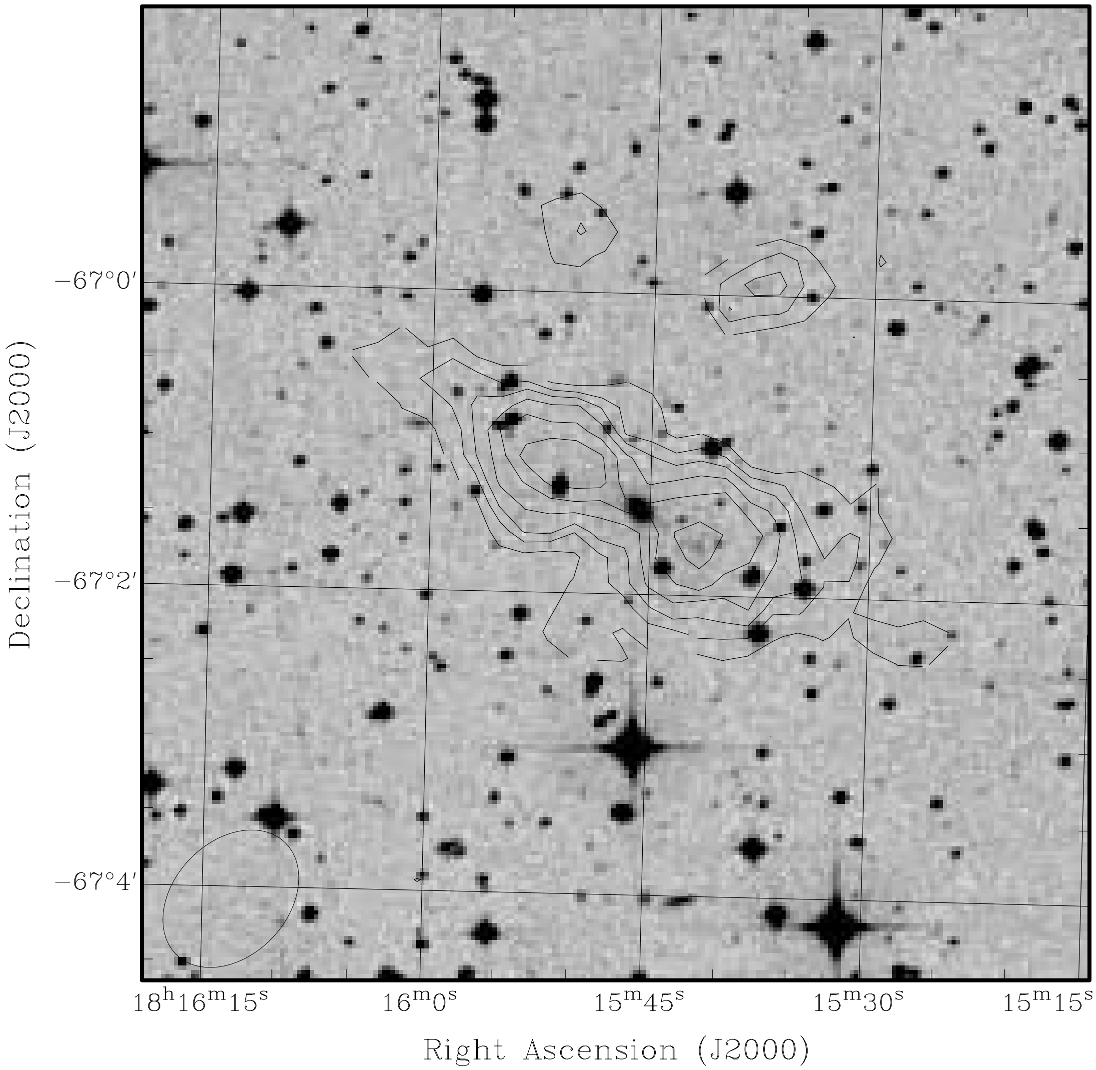

Fig. 14*b*

sky. The new galaxies mainly consist of optically faint galaxies, compact high surface brightness galaxies, and galaxies optically obscured by the Milky Way. A large H i cloud was detected near the galaxy NGC 2442, which does not seem to have any associated optical emission (Ryder et al. 2001). In addition a number of isolated H i clouds were found at velocities between 300 and 500 km s^{-1}, including the H i cloud HIPASS J1712-64 (Kilborn et al. 2000). It is uncertain whether these clouds are extragalactic or whether they are a product of the Magellanic Clouds–Galaxy interaction. A large percentage of the new galaxies lie along the Galactic plane, although a number of dwarf galaxies were discovered that were not in visually obscured regions. A couple of galaxies were found visually obscured by the Large Magellanic Cloud, which will be important for unbiased measurements of dust extinction in the Clouds (Dutra et al. 2001).

As mentioned in § 4, a number of these new galaxies have been observed at ATCA. In general, the galaxies chosen for observation were those with no obvious optical counterpart on the DSS images. Of those galaxies detected with ATCA, all apart from the previously mentioned HIPASS J1712-64 have optical emission associated with them. Two examples of new high surface brightness detections are shown in Figure 14. HIPASS J0305-69 consists of two H i clumps, with a compact optical counterpart associated with the larger clump. There is another compact optical counterpart for the smaller clump, but it is unclear whether this counterpart is a foreground star or emission associated with the galaxy. HIPASS J1816-67 has a very large H i disk surrounding the compact optical counterpart. In both these detections the optical counterparts are hardly more extended than the foreground stars, leading to them being missed in previous optical galaxy surveys. Four low-mass LSB galaxies were detected. These galaxies all have a smooth distribution of H i, with a faint optical counterpart lying in the highest column density region of their disks. The disks are typically 2 or 3 times the spatial size of the visible optical counterpart. The lowest-mass new galaxy detected was HIPASS J1247-77, which has an H i mass of 4.6×10^6 $M_{\odot}$ for an estimated distance of 2.2 Mpc. The ATCA synthesis image overlaid on the DSS I optical image is shown in Figure 15. This galaxy lies close to emission from the Magellanic Clouds and is also near the dwarf galaxy IC 3104, which lies at 430 km s^{-1}.

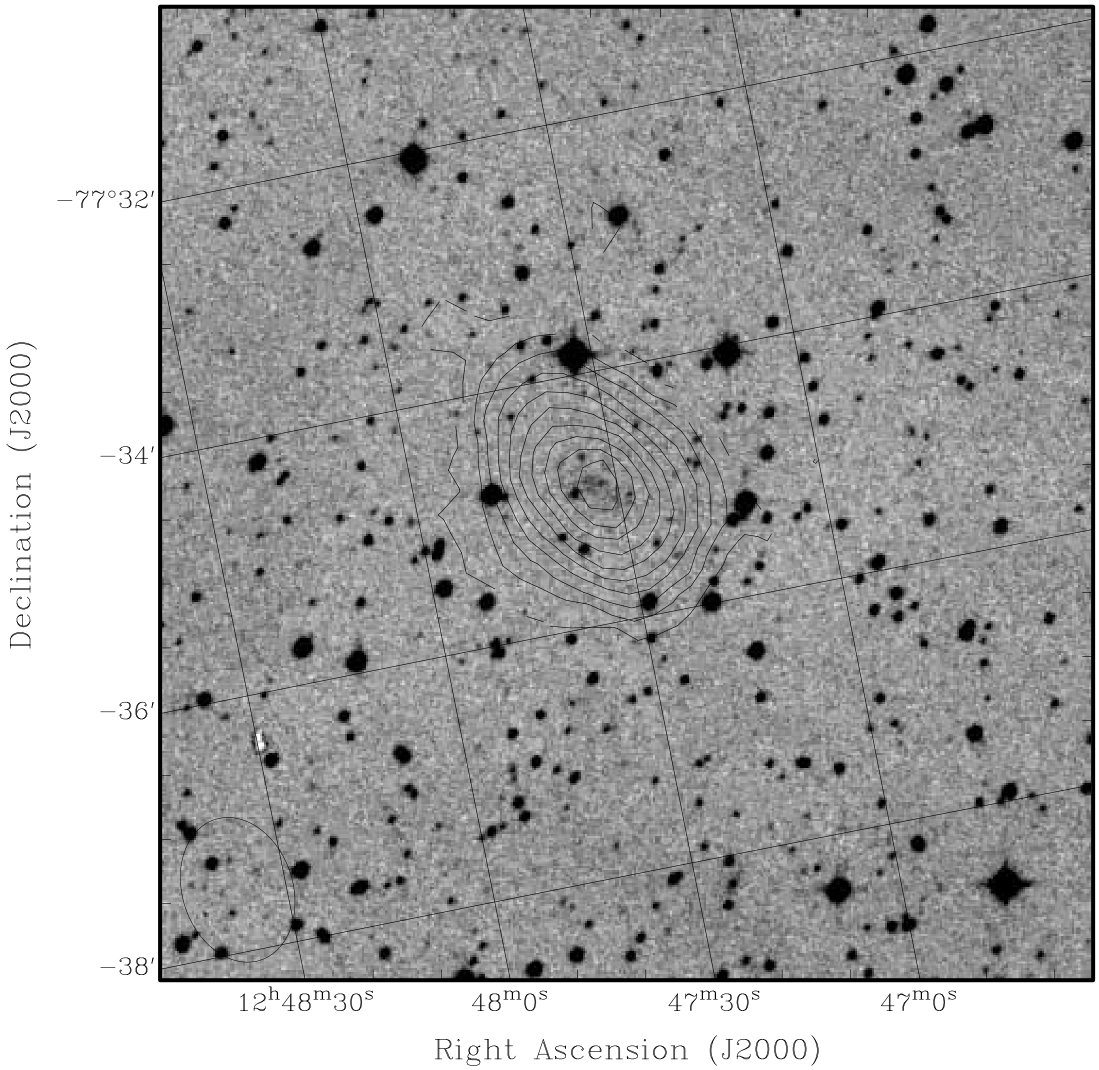

FIG. 15.—ATCA observation of a previously uncataloged low surface brightness galaxy, HIPASS J1247-77. This galaxy lies at a velocity of 411 km s^{-1} and has an H I mass of just 4.6 $\times\ 10^6\ M_\odot$ at the distance of 2.2 Mpc. The beam is shown at bottom left in the image.

9. SUMMARY

The SCC catalog allows the study of the H I content of galaxies free from any optical bias in the sample selection. The accuracy of HIPASS detections was determined using follow-up observations at ATCA. The positional rms from the ATCA observations was 1.′9. The H I selected galaxies followed the large-scale structure laid out by optical catalogs, although the number of H I detections in optical regions of high galaxy density was not high. The mass range of the sample is very large—from $\sim 5 \times 10^6$ to $\sim 9 \times 10^{10}$ $M_\odot$, which is the largest mass range from a blind H I survey of galaxies. The size of the catalog allows for the optical properties of the H I–rich galaxies to be studied. More late-type galaxies were found in the H I sample, with 58% of galaxies being either late spiral galaxies or late types, compared with 30% for the known optically selected galaxies in the same region. The H I mass-to-light ratio increased from a mean value of 1.8 for early-type galaxies to 3.2 for late types. The galaxies are much more gas-rich than typical values from optical samples.

Galaxies without previously cataloged optical counterparts generally had either an LSB counterpart nearby, were located near a bright star, or were in the optically obscured ZOA. A small number of H I clouds without optical counterparts was found, but these lay at low velocities, and it is unclear whether these are extragalactic H I clouds or HVCs that are associated with the Magellanic Clouds–Galaxy interaction. From the number of galaxies detected in this region, we predict that the full survey will contain in excess of 5000 galaxies, down to a peak flux limit of 39 mJy. This number is a lower limit, as the presented catalog is likely to be incomplete at this flux level, and with improved galaxy detection algorithms the final catalog should be more nearly complete. In addition there were two voids in the SCC region, the Sculptor and Eridanus voids, which have possibly resulted in fewer detections in this region than in HIPASS on average.

We would like to thank the staff at the Parkes observatory for their support throughout the observations and the ZOA team for help with HIPASS observations. We are grateful to S. Gurovich, S. Mader, J. Stevens, and M. Zwaan for providing details about narrowband confirmation observations. Thanks also to the referee for helpful remarks. V. Kilborn acknowledges support from an Australian Postgraduate Award.

REFERENCES

Allen, R. J. 2001, in ASP Conf. Proc. 240, Gas and Galaxy Evolution, ed. J. E. Hibbard, M. P. Rupen, & J. H. van Gorkom (San Francisco: ASP), 331
Banks, G. D., et al. 1999, ApJ, 524, 612
Barnes, D. G. 1998, Ph.D. thesis, Univ. Melbourne
Barnes, D. G., et al. 2001, MNRAS, 322, 486
Boyce, P. J., et al. 2001, ApJ, 560, L127
Carignan, C. 1999, Publ. Astron. Soc. Australia, 16, 18
Davé, R., et al. 2001, ApJ, 552, 473
Disney, M. J. 1976, Nature, 263, 573
Duprie, K., & Schneider, S. E. 1996, AJ, 112, 937
Dutra, C. M., Bica, E., Clariá, J. J., Piatti, A. E., & Ahumada, A. V. 2001, A&A, 371, 895
Fairall, A. 1998, Large-Scale Structures in the Universe (New York: Wiley)
Giovanelli, R., & Haynes, M. P. 1985, ApJ, 292, 404
Gooch, R. 1995, in ASP Conf. Ser. 77, Astonomical Data Analysis Software and Systems IV, ed. R. A. Shaw, H. E. Payne, & J. E. Haynes (San Franciso: ASP), 144
Haynes, M. P., Giovanelli, R., & Chincarini, G. L. 1984, ARA&A, 22, 445
Henning, P. A., et al. 2000, AJ, 119, 2686
Hoffman, G. L., Williams, B. M., Lewis, B. M., Helou, G., & Salpeter, E. E. 1989, ApJS, 69, 65
Huchtmeier, W., & Richter, O. 1989, A General Catalog of H I Observations of Galaxies (Berlin: Springer)
Huchtmeier, W. K., Hopp, U., & Kuhn, B. 1997, A&A, 319, 67
Impey, C. D., & Bothun, G. D. 1997, ARA&A, 35, 267
Juraszek, S. J., et al. 2000, AJ, 119, 1627
Kilborn, V. A. 2001, Ph.D. thesis, Univ. Melbourne
Kilborn, V. A., et al. 2000, AJ, 120, 1342
Kilborn, V. A., et al. 2002, in preparation
Kraan-Korteweg, R. C., & Tammann, G. A. 1979, Astron. Nachr., 300, 181
Marquarding, M. 2000, Master's thesis, Univ. Melbourne
Mathewson, D. S., Ford, V. L., & Buchhorn, M. 1992, ApJS, 81, 413
Oosterloo, T., & Morganti, R. 2001, in ASP Conf. Proc. 240, Gas and Galaxy Evolution, ed. J. E. Hibbard, M. P. Rupen, & J. H. van Gorkom (San Francisco: ASP), 251
Putman, M. E., et al. 2002, AJ, 123, 873
———. 1998, Nature, 394, 752
Rao, S., & Briggs, F. 1993, ApJ, 419, 515
Rosenberg, J. L., & Schneider, S. E. 2000, ApJS, 130, 177
Ryder, S. D., et al. 2001, ApJ, 555, 232
Sadler, E. M. 1997, Publ. Astron. Soc. Australia, 14, 45
Sandage, A., & Bedke, J. 1994, The Carnegie Atlas of Galaxies (Washington: Carnegie Inst. Washington)
Smith, D. A., Allen, R. J., Bohlin, R. C., Nicholson, N., & Stecher, T. P. 2000, ApJ, 538, 608
Solanes, J. M., Giovanelli, R., & Haynes, M. P. 1996, ApJ, 461, 609
Solanes, J. M., Manrique, A., Garcia-Gomez, G., Gonzalez-Casado, G., Giovanelli, R., & Haynes, M. P. 2001, ApJ, 548, 97
Sorar, E. 1994, Ph.D. thesis, Pittsburgh Univ.
Spitzak, J. G., & Schneider, S. E. 1998, ApJS, 119, 159
Staveley-Smith, L., Davies, R. D., & Kinman, T. D. 1992, MNRAS, 258, 334
Tantisrisuk, S., et al. 2002, in preparation
Valluri, M., & Jog, C. J. 1991, ApJ, 374, 103
Wakker, B. P., & van Woerden, H. 1991, A&A, 250, 509
Waugh, M., et al. 2002, MNRAS, submitted